ACS APPLIED NANO MATERIALS
Cite This: ACS Appl. Nano Mater. 2019, 2, 4594−4604
Article
www.acsanm.org

Post-Growth Planarization of Vertically Aligned Carbon Nanotube Forests for Electron-Emission Devices

Mohab O. Hassan,[†,‡] Alireza Nojeh,*[,†,‡] and Kenichi Takahata*[,†]

[†]Department of Electrical and Computer Engineering, University of British Columbia, Vancouver, British Columbia V6T 1Z4, Canada

[‡]Quantum Matter Institute, University of British Columbia, Vancouver, British Columbia V6T 1Z4, Canada

Supporting Information

ABSTRACT: This paper reports a microplasma-based planar process for as-grown carbon nanotube (CNT) forests to produce macroscopically flat top surfaces over different scales. This noncontact process is based on microscale removal of CNTs driven by pulsed electrical discharge generated at the interface between the forest surface and a stainless-steel planar electrode, achieving controlled subtractive planarization of the forest structure while maintaining the CNTs' alignment. Forest samples with large surface areas of up to 26 mm^2 with the largest height variations of ∼1 mm are successfully processed to demonstrate improvements by up to ∼60× in the height uniformity of the forests and ∼30× in the parallelism of their top surfaces with the substrate planes. Elemental analyses suggest that the contamination from the electrode material is minor, or negligibly small when the discharge process does not experience short-circuit events that can lead to damaging irregular arcs. The promising results obtained in this work are expected to pave the way for studying the properties of the CNT forest further and promote its application in areas where height uniformity is of prime interest, such as in electron emission devices.

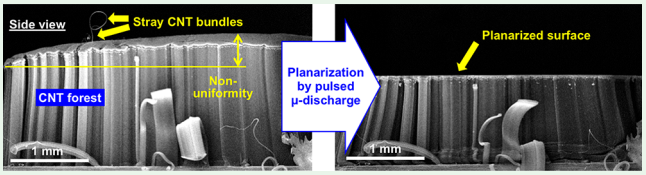

KEYWORDS: *carbon nanotube forest, planarization, micromachining, pulsed electrical discharge, growth uniformity, scaling effect*

1. INTRODUCTION

Carbon nanotubes (CNTs) are attracting significant attention due to their unique electrical, optical, mechanical, and chemical properties.[1−6] They can be synthesized or grown in many forms. The CNT forest, an array of individual CNTs aligned vertically on their substrate, is one of the forms that offer unique physical and electronic features.[7−10] It can be grown on a substrate with a predeposited catalyst that initiates the growth process at high temperatures by chemical vapor deposition (CVD).[11−13] The localized growth of CNT forests can be controlled through prepatterning of the catalyst layer on their substrates prior to the growth process.[10,14−16] This pregrowth fabrication process allows for lateral control over the growth sites. However, there is a less control over the vertical direction of the growth. This typically results in relatively large nonuniformities on the top surfaces of grown CNT forest structures, where stray CNT bundles can be randomly found on these surfaces, affecting the structural precision and integrity of the forests.[17−19] Moreover, the uniformity of CNT forests is typically compromised when grown on relatively large substrates (with surface areas of a few mm^2 or greater).[15,20] Estimated values of height deviation across the top surface of CNT forest structures found in the literature are in the range of 34.8−689.8 μm/mm^2.[15,16,20,21] The nonuniformity of the grown height can result from several factors, including the nonuniformity in the growth catalyst itself, the spatial variation of process temperature, and the variation of local partial pressure of the precursor gas.[16] The forest's nonuniformity can also be related to the spatial distribution of the catalyst nanoparticles on the substrate, which in turn impacts the mechanical coupling between neighboring CNTs during the growth process and eventually affects the overall uniformity.[21] A high uniformity in the height of the CNT forest is crucial in understanding basic electrostatic characteristics such as the capacitance.[22] Several studies have shown the integration of CNT forests with micro-electromechanical systems (MEMS) devices such as supercapacitor electrodes,[23,24] highly durable electrodes,[25] and electrostatically actuated varactors.[26] Another important application where the uniformity of CNT forests becomes vital is thermionic and field-emission devices. For example, a recent discovery has revealed a unique property of CNT forests as a strong candidate for the cathode material in thermionic energy conversion devices.[27] In this type of devices, the gap between the cathode (CNT forest in this case) and the anode should be ideally on the order of a few micrometers for efficient collection of the emitted electrons.[28] This has been a challenge in previous studies, which could only use gaps on the order of a millimeter due to the nonuniformity in the CNT forest structures used.[29−31] The presence of stray CNT bundles emerging from the top of the forest is also a critical problem as it can cause short circuits with the anode.

Received: May 21, 2019
Accepted: June 21, 2019
Published: June 21, 2019

DOI: 10.1021/acsanm.9b00948
ACS Appl. Nano Mater. 2019, 2, 4594−4604

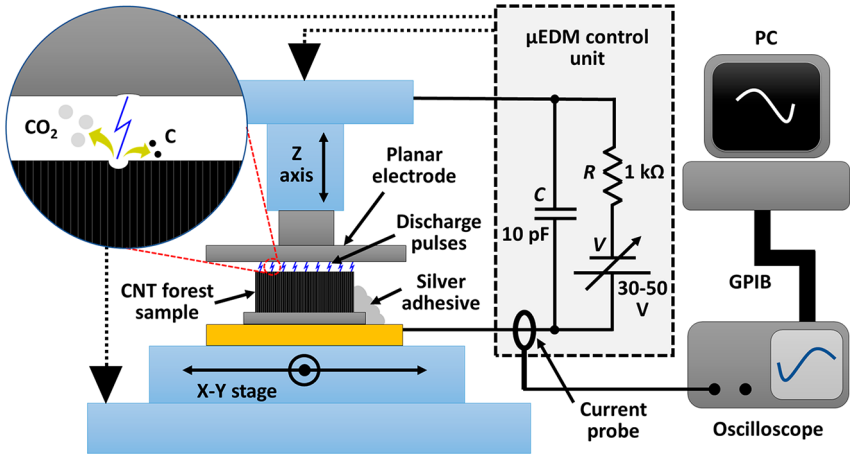

Figure 1. Experimental setup for μEDM planarization of CNT forests using a planar electrode in a 3-axis numerical control system. An inductive current probe is coupled with the discharge circuit for measurement of pulse amplitude and timing, whose signals are captured and recorded by a computer.

Two approaches can be followed to address the inherent uniformity problem in the CNT forest, namely bottom-up and top-down approaches. The bottom-up approach is a pre- or during- growth technique to tackle the issue. It relies mainly on optimizing and controlling different aspects of the growth catalyst itself as well as the growth conditions. However, the effectiveness of this approach has been limited. For example, a study of the population growth dynamics of CNT forests has shown that it is generally difficult to experimentally produce uniform and millimeter-scale tall CNT forests over large areas.[32] Another experimental study that focused on controlling the gas flow direction during the growth process has shown large area growth of CNT forests but without improving the surface uniformity.[33] Theoretical studies of spatially dependent CNT forest growth have shown promising results toward achieving uniform CNT forests by controlling the size and spacing of the catalyst patterns; however, they have not demonstrated the effects experimentally.[15] The top-down approach relies on postgrowth techniques, to free-form pattern the entire CNT forest structure as a whole unit. This includes the removal of undesired structural nonuniformity and stray CNT bundles from their top surfaces. There have not been many reports that demonstrate this approach. In one study, a pulsed laser has been used to etch patterns on a CNT forest top surface.[34,35] This technique, however, has limitations in geometrical/dimensional controllability (e.g., slope on the sidewalls and accuracy in depth control). Another method is the densification of CNT forest structures.[36,37] This method can achieve three-dimensional (3D) micropatterns; however, it requires prepatterning of the growth catalyst. Among the previously reported top-down techniques, the micro-electro-discharge machining (μEDM) technique[38] seems to be one of the promising methods for postprocessing of CNT forests in terms of precision and geometrical freedom for the process. μEDM is a microplasma-based technique that uses pulses of thermomechanical impact induced by miniaturized arc discharges that are generated between a microscale electrode and a workpiece. This allows for localized and controlled removal of the workpiece material depending on the size/shape of the electrode. Being able to etch any electrically conductive material, μEDM has been a powerful tool for the micromachining of bulk metals and alloys for a variety of applications, including MEMS and precision engineering.[38−42] Moreover, the numerical position control of both electrode and workpiece in μEDM enables 3D patterning with high precision.[43] This technique has been demonstrated to be highly effective for micropatterning of CNT forests as well.[44−46] With its noncontact, microplasma-based principle, it can locally evaporate and remove individual CNTs while maintaining their alignment in a forest form. Several studies have evaluated μEDM parameters in patterning CNT forests.[44,47−50] Microscale 3D shaping in CNT forests has been enabled with the nanoprecision numerical control capability of the process.[45,51] Unlike conventional μEDM, in which a dielectric liquid serves as the processing medium, the reported μEDM-based CNT forest patterning has used gas ambients, including air[47] and oxygen-mixed sulfur hexafluoride,[52] because the CNTs in a forest collapse and lose their alignment when being dried after wet processing.[47] This dry μEDM was reported to be driven by thermally enhanced oxidation of CNTs, working essentially as a pulsed local oxygen plasma etching of the nanotubes.[55]

In this report, a microscale process for postgrowth planarization of CNT forests is investigated with a focus on the use of the μEDM principle. In particular, the nonuniformity in the CNT forests grown to have millimeter-scale heights is addressed through the use of planar electrodes in the pulsed discharge process (Figure 1), unlike previous studies that used single-tip, micro cylindrical electrodes for CNT forest processing. The process and setup parameters for the planar μEDM removal of the CNT forest including the applied voltage, lateral motion of the electrode, and electrical contact method are varied to assess and optimize the flattening process. The scalability of the process is investigated using CNT forests with relatively large areas, showing promising results in their height uniformity and surface smoothness. The achieved process and obtained results are expected to facilitate the application of CNT forests in a variety of areas including MEMS, microelectronics, and thermionic energy conversion.

2. EXPERIMENTAL METHODS

2.1. CNT Forest Growth. The CNT forest samples used in this study are grown on highly doped silicon substrates (resistivity 0.002−0.005 Ω·cm) using a hot-wall atmospheric-pressure chemical vapor deposition (CVD) system. The catalyst deposited on these substrates is iron with an alumina support layer, with thicknesses of 1.1 and 10

DOI: 10.1021/acsanm.9b00948
ACS Appl. Nano Mater. 2019, 2, 4594−4604

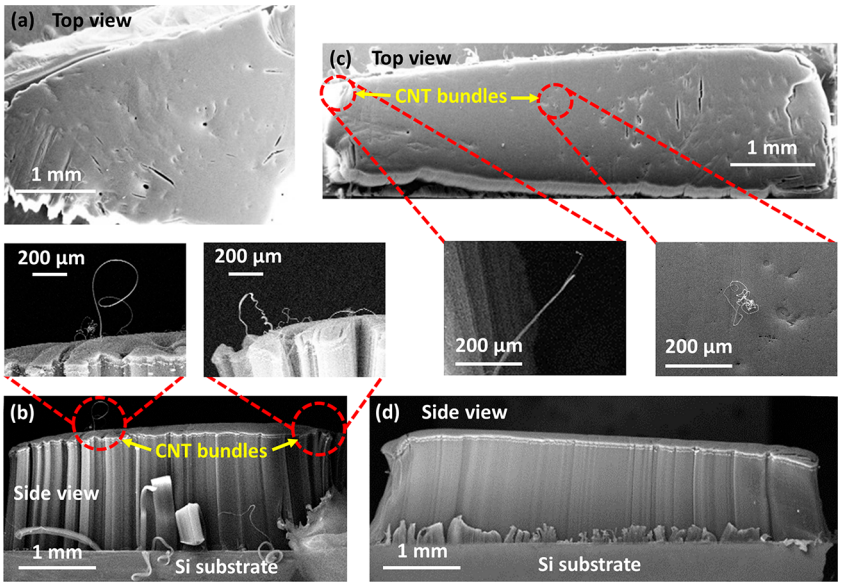

Figure 2. SEM images of CNT forest samples grown using the CVD method: (a) Top and (b) side views of sample no. 1; (c) top and (d) side views of sample no. 2. The close-up insets in (b) and (c) show stray CNT bundles sticking out of the top surfaces of these CNT forests.

nm, respectively. The process is performed in the mixture of argon, hydrogen, and ethylene that acts as the carbon-containing active precursor for the growth of the CNT forests at a temperature of 750 °C. More details about the growth process can be found in other reports.[31,53] One method to control the height of the CNT forest is to vary the growth time, that is, the time period for which ethylene is flowed through the CVD growth chamber. The growth time chosen for this study is 40 min, which results in CNT forests of 1 mm or greater in height. The grown height of the forest also appears to depend on the size of the substrate, where smaller ones generally show higher growth rates. Height variations are present in almost all substrates even those with the same size.

2.2. Sample Preparation. The electrical connection to a grown CNT forest is made using one of two means, a conductive adhesive (Silver Paste Plus 05063-AB, SPI supplies, PA), and a clamped copper wire (with 320 μm in wire diameter), each of which is applied directly to the forest structure. For the silver adhesive, it is carefully applied to a side of the CNT forest so that it only touches the bottom part of the forest's side wall. This is to ensure that the largest height of the adhesive (after curing) is sufficiently lower than the actual height of the CNT forest so that discharging cannot occur with the adhesive itself during the μEDM process. The other contact method is implemented by clamping the copper wire to a sidewall of the CNT forest. In this case as well, the height of the copper wire is adjusted to be lower than that of the CNT forest to avoid discharging with the wire instead of with the forest.

2.3. μEDM Planarization Process. The planarization process of CNT forest samples is conducted using a commercially available μEDM system (EM203, SmalTec International, IL). The experimental setup is illustrated in Figure 1. The system has X-Y and Z stages, each of which has a 100 nm positioning resolution. The electrode is held on the Z stage while the workpiece is fixed to the X-Y stage. A piece of 200-μm-thick stainless-steel flat sheet with a size of 25 × 25 mm^2 serves as the planar electrode for the flattening process. The electrode is directly mounted on the bottom surface of the Z stage to ensure that the electrode plane is parallel with the X-Y stage of the system. In this study, all the μEDM processes are performed in air that acts as the dielectric material between the electrode and the forest sample.[44,45,47,51] The system uses a relaxation type resistor-capacitor (R-C) circuit that serves as a discharge pulse generator. The energy of a single discharge pulse, E, is given by $(C + C')V^2/2$, where C is the capacitance chosen for a specific process, C' is the total parasitic capacitance in the system including the capacitance present between the electrode and the workpiece (CNT forest), and V is the voltage applied between them. The component of C' that comes from the system itself is small, typically around 10 pF. However, C' associated with the parallel set of the planar electrode and the CNT forest is unknown and will be discussed later.

The main μEDM process parameters are V, C, and the feeding/scanning rates of the Z and X-Y stages. The discharge energy is varied with V while maintaining a constant C of 10 pF. The stages' motion rates are varied and optimized for the flattening process. The polarity of V is chosen so that the CNT forest is positive, whereas the planar electrode is negative, the polarity used in typical μEDM. The Z stage that holds the planar electrode is fed toward the top surface of the workpiece at a constant rate of 10 μm/min. This rate, lower than typical values used in the reported μEDM of CNT forests using microscale cylindrical electrodes,[47] is selected by considering the substantially larger machining areas involved in the current study that uses planar electrodes. In certain cases, the forest sample is scanned along the X direction (with a rate of 10 mm/min for a distance of 1 mm) in a reciprocating manner under the planar electrode in order to observe its influence on the planarizing effect. In case of a short circuit event, the system is configured to automatically stop all motions and retract the electrode upward to clear the short, after which the electrode is lowered to resume the discharge process. For all processes, the planar electrode is fed down through two steps in this study. The main purpose of the first step is to remove any stray CNT bundle sticking out of the top surface of the CNT forest (Figure 2). The feeding distance in this step is chosen to be 200 μm based on an estimate of the height of those CNT bundles. The electrode keeps moving toward the sample to initiate discharge pulses on the forest's top surface. The second step is implemented to define the removal depth in the CNT forest that is greater than or equivalent to the maximum height variation present on the top surface, for the purpose of flattening. The feeding distance for this second step is set to be 500 μm to remove the entire variation present on the top surfaces of the CNT forests (refer to Table 1) prepared in this study (except for sample no. 3 whose variation was greater than 500 μm as in the table).

2.4. Process and Material Characterizations. The pulsed discharge currents generated during the process are quantified using an inductive current probe (CT-1, Tektronix Inc., OR) that is inserted into the R-C circuit (Figure 1) and monitored through an oscilloscope (TDS 2012, Tektronix). A GPIB connection is established between the oscilloscope and a computer to store the discharge current data for further analysis.

For structural and surface characterizations of as-grown and μEDM-processed CNT forests, a scanning electron microscope

DOI: 10.1021/acsanm.9b00948
ACS Appl. Nano Mater. 2019, 2, 4594−4604

Table 1. CNT Forest Samples Used for Planarization Experiments

sample no.	height (mm)	top surface area (mm^2)	nonuniformity	
			overall tilt (deg)	maximum height variation (mm)
1	1.72	8.00	3.62	0.45
2	1.51	6.13	3.14	0.52
3	~2	26.01	not applicable	~1.1
4	1.74	10.01	1.32	0.32

(SEM; Zeiss Sigma, Carl Zeiss NTS GmbH, Germany) is employed in this study. It is used to examine the samples after the growth process to determine the initial height, quality and nonuniformity on the top surfaces of as-grown samples, as well as those of the postprocessed samples for comparison. It should be noted that other surface characterization techniques such as profilometery or atomic force microscopy (AFM) were found inadequate to assess and characterize the CNT forest top surface. The profilometer's tracking force was found to be high such that it did not detect the top surface and caused damages, and the AFM scanning range was too small (a few tens of micrometers) to assess the flatness of large surfaces (a few mm^2). The current study evaluates the planarization effect by comparing the following two parameters with those from the as-grown form: (1) height variation of the forest structure over the processed top surface area, and (2) tilt angle (parallelism) of the processed top surface with respect to its substrate (in case there is a consistent overall angle on the forest's top surface). On the same SEM system, energy-dispersive X-ray spectroscopy (EDX; with an electron beam energy of 10 keV) is conducted on the μEDMed forest surfaces. This EDX analysis is specifically intended to quantify elemental signatures of the μEDM electrode's material that could be present on the forest's surfaces due to the wear of the electrode and any other contamination left on the surfaces after the removal process.

3. RESULTS AND DISCUSSION

3.1. CNT Forest Growth and Interface with Discharge Circuit. Four of the CNT forest samples grown and used for the current study are listed in Table 1 along with their heights (measured from the substrate surface to the highest point on the sample) and the top surface areas. As shown, every sample showed a large nonuniformity in its height. An overall slope present on the entire top surface was also measured and included in the table for each sample (except for sample no. 3, in which this was difficult to quantify due to inconsistent height variation). Top and side SEM images of the as-grown structures of the first two samples are shown in Figure 2. Sample no. 3, with its 3−4× larger area than sample nos. 1 and 2, was used to observe the scaling effects of the planarization process. Besides the sloped top surface, most of the samples showed random stray CNT bundles sticking out of or lying on the top surfaces of them (see insets in Figure 2b,c), which constitute another type of defects to be removed via the flattening process.

The contact resistance to a CNT forest sample, made through either the silver adhesive or the copper wire clamp, was characterized in separate experiments by measuring the electrical resistance between the contact material and a metallic probe placed on the forest's top surface. The resistance was found to be less than 100 Ω with three random samples for each type of the contact, which was a satisfactory level for μEDM according to previous reports.[46,47]

3.2. Planarization Process and Analysis. The applied voltage was varied to define its lowest level that was sufficient to sustain discharge pulses with the defined capacitance (10 pF) and feeding rate (10 μm/min) while achieving high quality surfaces with a minimal discharge energy. The voltage was raised starting from 30 V, based on those used in previous studies,[46,47] until reaching the above discharge condition, and the minimal voltage level that fulfilled the condition was found to be ~50 V. Given this result, the following experiments consistently used 50 V as the machining voltage. The μEDM process parameters used for processing each sample are listed in Table 2.

Table 2. μEDM Process Parameters Applied for Prepared CNT Forest Samples

sample no.	voltage, capacitance, electrode feed rate	sample lateral motion rate	removal depth	electrical connection
1	50 V, 10 pF, 10 μm/min	10 mm/min	500 μm (excluding initial ~200-μm feed for stray CNT removal)	silver adhesive
2		stationary		copper wire
3		stationary		silver adhesive
4		10 mm/min	not applicable	copper wire

The μEDM process for sample no. 1 with its lateral motion was observed to be highly stable with no detection of short circuit events. The debris produced in this removal process tended to be left on the surface of the electrode (the dark area in Supporting Information (SI) Figure S1a). Depending on the level of nonuniformity in the original sample, in fact, the part of the electrode at which the discharge pulses took place seemed to accumulate the debris and affected the stability of pulse generation with enhanced short circuit events toward the end of the process. The SEM observation of the electrode's surface indicated crater-like marks created by discharge pulses, suggesting a certain level of consumption that occurred on the electrode. The profile measurement using a stylus profilometer (DektakXT, Bruker Co., MA) revealed that this consumption was minor, with a depth of 1−1.5 μm.

For sample no. 2 with the wire contact, the same process parameters were applied, except for the electrode's lateral motion that was removed in this case. During the 500 μm electrode feed, frequent short circuit events occurred and resulted in stalling the removal process, unlike the process for sample no. 1. It was observed that a significant amount of debris was left on both the forest surface and the machining region of the electrode. Consequently, the location of the electrode was changed to use a debris-free area over the electrode's surface, which was repeated two times (SI Figure S1b) to complete the entire 500 μm feed depth. The profile measurement of the electrode showed a similar consumed depth (1−1.5 μm) for each of the three locations used for the process (i.e., the total electrode wear was approximately three times the amount seen with sample no. 1). The main reason behind this outcome led by short circuits is presumed to be the lack of the electrode's lateral motion, which could have assisted to cut irregular continuous arcing.[46,54] This arcing could have also enhanced the production of substantial debris as well as the electrode consumption. Another potential factor may be related to the electrical contact with the wire clamp, which could have had an increased contact resistance (due to, e.g., weakened contact pressure) to cause energy loss at the contact

DOI: 10.1021/acsanm.9b00948
ACS Appl. Nano Mater. 2019, 2, 4594−4604

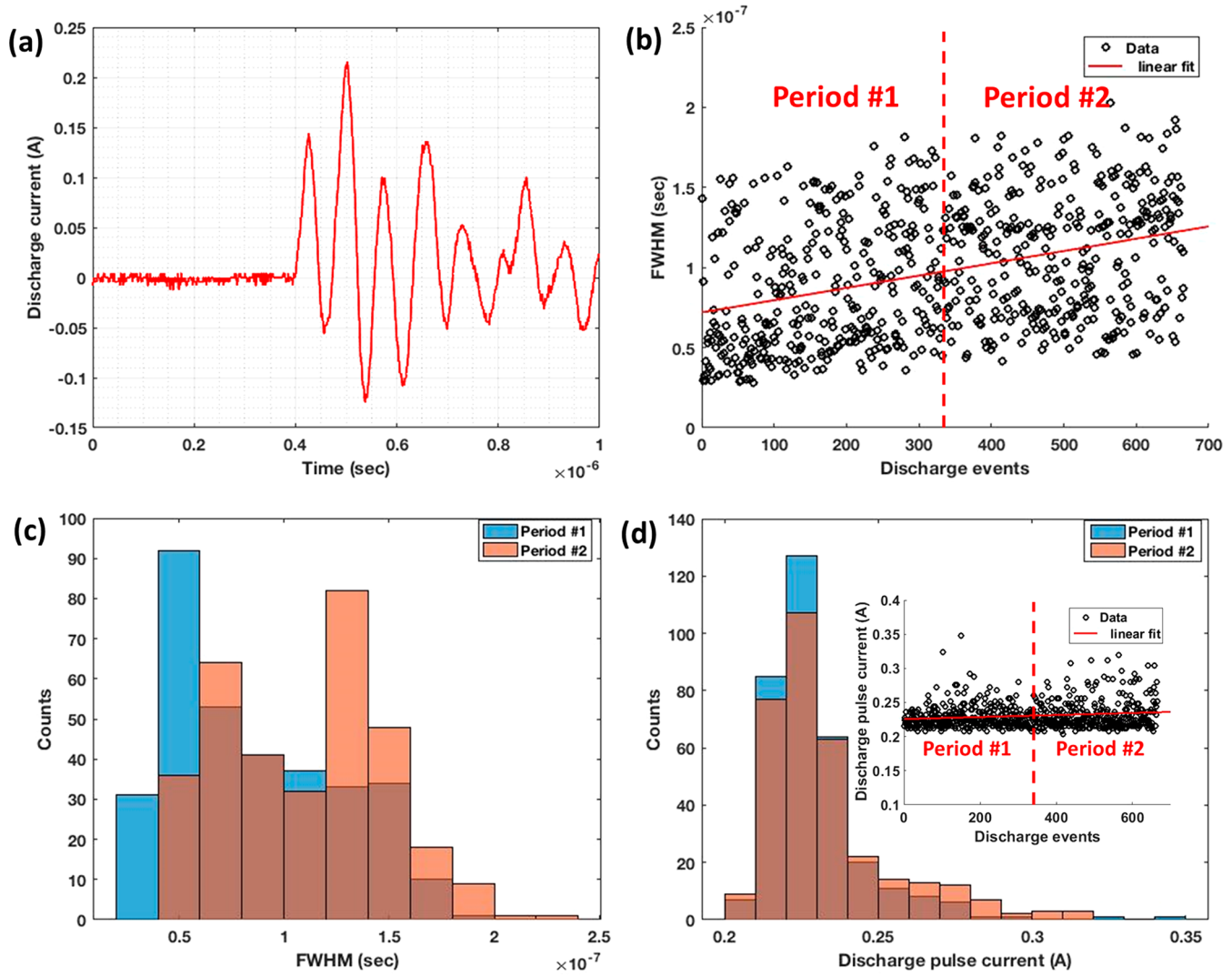

Figure 3. μEDM characteristics obtained from sample no. 3 flattening: (a) An example of single discharge current pulse; (b) a temporal plot of the measured fwhm of the discharge pulses captured throughout the process (each data point acquired every ∼4 s) and their average trend; (c) a plot of the fwhm for the two periods shown in (b); (d) a plot of the peak discharge current for the two periods (the inset shows a temporal plot of the peak current captured throughout the same process (with the same data collection interval)).

while the process was in progress, lowering the discharge energy and negatively impacting the removal process.

For sample no. 3, its electrical connection was made with the silver adhesive considering the potential instability with the wire clamping method. The discharging process was characterized using this sample with the setup as discussed in Section 2. An example of measured discharge pulse is displayed in Figure 3a, showing the peak pulse current of 216 mA. This current level is consistent with the previous result under a similar μEDM condition (with the normal voltage polarity same as the current study).[47] The pulse width (full width at half-maximum, or fwhm) and peak current of the discharge were tracked for the entire process time (∼50 min, through the second feed step—refer to Section 2) and plotted in Figure 3b,d, respectively. It should be noted that in this data collection, there was a ∼4 s interval between two adjacent collection timings (to cover the entire process period, while limiting the data within a manageable range). The tracked trend of the fwhm (Figure 3b) indicates a noticeable increase along the process time, with an average rate of +77 ps per collection interval. To analyze this trend further, the process time was divided into two equal periods as shown in Figure 3b, and the pulse counts were plotted with varying fwhm levels for the two periods in an overlaid manner in Figure 3c. This plot shows that the fwhm was centered at ∼50 ns in period no. 1 and then shifted toward ∼130 ns in period no. 2. The measured peak discharge current tracked and plotted in a similar manner as the fwhm is shown in Figure 3d. It can be seen that the peak current was centered at ∼225 mA throughout the process; however, while moving from period nos. 1 and 2, there was a consistent decrease in the number of pulses with lower values (200−250 mA) whereas an increase in that with higher values (250−350 mA). Although the trend of peak current did not appear to be as significant as that of the fwhm, the measurement results indeed indicated an increasing trend (of 14.8 μA per collection interval) during the process.

Since sample no. 3 was highly nonuniform, the deeper the electrode went into the surface, the larger the interface area between the electrode and the CNT forest top surface became. (This is presumably the reason that the process experienced several short circuit events toward the end of the feed.) This means that as removal proceeds, the capacitance between the

DOI: 10.1021/acsanm.9b00948
ACS Appl. Nano Mater. 2019, 2, 4594−4604

planar electrode and the CNT forest, and thus the single discharge energy, could increase. The increase in the pulse energy can result in the enlargements of both the pulse width and peak current. This hypothesis matches well with the above-mentioned observation. This consequently means that the parasitic capacitance induced at the interface between the planar electrode and the CNT forest might not be negligible for the process. According to an electrostatic study of the top surface of the CNT forest (defined as micropillar structures), the numerically calculated capacitance with a counter electrode was ~1 fF at a few micrometers of gap for an approximate effective area of 3×10^{-3} mm^2.[22] Scaling the area to match that of sample no. 3 (26 mm^2) suggests a capacitance of ~8.67 pF, which is, in fact, comparable to the estimated parasitic capacitance (10 pF) of the μEDM system itself.

3.3. Characterization of Planarized CNT Forests. The top and side view of sample no. 1 after μEDM planarization are shown in Figure 4a,b, respectively. The side view of the CNT forest visually indicates significant improvement of the top surface flatness compared with its pristine form. A SEM inspection located no stray CNT bundles present on the top surface. The tilt angle in the top surface with respect to the silicon substrate was found to be 0.48°, representing a parallelism improvement by ~7.5× from that of the as-grown sample (Table 1). This tilt can be translated into a height variation rate of 4.96 μm/mm^2 on the top surface, or a total postflattening variation of 39.7 μm over the entire top surface (with the total area of 8.00 mm^2). Given the original height variation (~450 μm) over the entire top surface, the result suggests a height uniformity improvement by ~11.3×. The close-up image of the top surface (near its edge, the close-up inset of Figure 4b) shows a surface roughness (estimated to be in the range of a few micrometers), with random pits likely caused by concentrated discharge pulses having occurred at these locations; however, the integrity and orientation of the CNTs inside the forest were not altered after the planarization process. The processed top surface appeared to show slight bending of the CNT tips and their aggregation into bundles (Figure 4a, bending direction indicated with yellow lines in the inset). The bending was likely related to the lateral movement of the CNT forest sample under the electrode given the match of the bending direction with the motion's direction (Figure 4a inset), whereas the bundling effect could have been induced by the discharge process itself as reported previously.[46,55] Although there was a gap clearance (i.e., discharge gap) between the electrode and the forest's top surface, the debris present at the interface could have been dragged together with the relative motion of the electrode to exert a shear force on the tips of the CNTs and cause their bending.

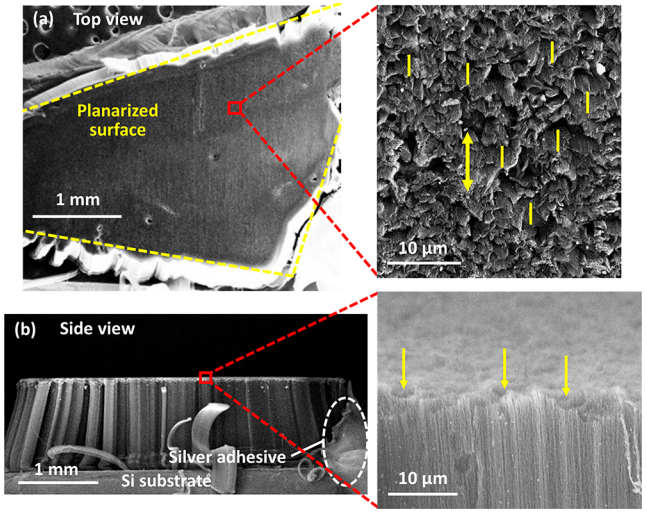

Figure 4. Planarization results for sample no. 1: (a) The top and (b) side views of the sample. The close-up insets in (a) and (b) show detailed texture of the top and side surfaces of the sample, respectively. The yellow arrow in the inset in (a) represents the electrode scanning direction, and the yellow lines represent the direction of CNT tip bending. The yellow arrows in the inset in (b) show the random pits present on the forest top surface.

The overall tilt on the top surface of the flattened sample no. 2 (Figure 5) was measured to be 0.1°, or a height variation rate of 1.38 μm/mm^2 over the entire surface, suggesting improvements in the parallelism and height uniformity by ~31.4× and ~61.5 × , respectively. The surface characteristics of this sample were found to be similar to those of sample no. 1 in terms of the surface roughness level and the bundling effect, except that there was no apparent sign of bending of the CNTs' tips. As the process for this sample was conducted with the stationary electrode, the outcome without the bending effect backs the previous hypothesis made with sample no. 1 that related it with the lateral motion of the electrode. In this sample, a significant amount of debris was found around the middle part of the forest's top surface (site no. 2 in Figure 5a). The main reason for this could also be related to the absence of lateral motion for the electrode, which presumably enhanced occurrence of irregular arching around the corresponding region leading to more production of debris in the region. It has been reported for μEDM of CNT forests that oxygen, necessary to drive local microplasma etching of CNTs,[55] could be depleted in the discharge space to cause frequent short circuits when using a planar electrode.[46] This circumstance, whose likelihood is more around the middle region of the forest rather than its perimeter, might be the case for the current process for sample no. 2 without the lateral motion that could facilitate the supply of fresh air (oxygen) to the discharge region, and thereby might have induced more irregular arcs and resultant debris. Nevertheless, these debris particles are known to be easily removable (by blowing nitrogen to the sample) without causing damages to the forest structures.[47]

In the process for sample no. 3, although the feeding depth of 500 μm was not sufficient to completely flatten the entire top surface of the forest given the large height variation of this particular sample (i.e., the lowest height regions near the edges of the forest were unexposed to discharge pulses), the feed was large enough to cover most of the surface area necessary to evaluate the process. As can be seen in Figure 6, this large forest structure was well flattened after the process, exhibiting a tilt angle of 0.61° with respect to the substrate, or a height variation rate of 3.22 μm/mm^2 (where the machining reached). Given the fact that the height variation removed in the machining was approximately equal to its feeding depth of 500 μm (as there was still a remaining variation that this feed did not reach), an improvement in the height variation can be estimated to be 6.0 ×. A summary of planarization results from sample nos. 1−3 is presented in SI Table S1.

The results from the EDX elemental analyses on the top surfaces of the processed three samples are shown in Figure 7. For sample nos. 1 and 3, the main identifiable peaks are C K, O

DOI: 10.1021/acsanm.9b00948
ACS Appl. Nano Mater. 2019, 2, 4594−4604

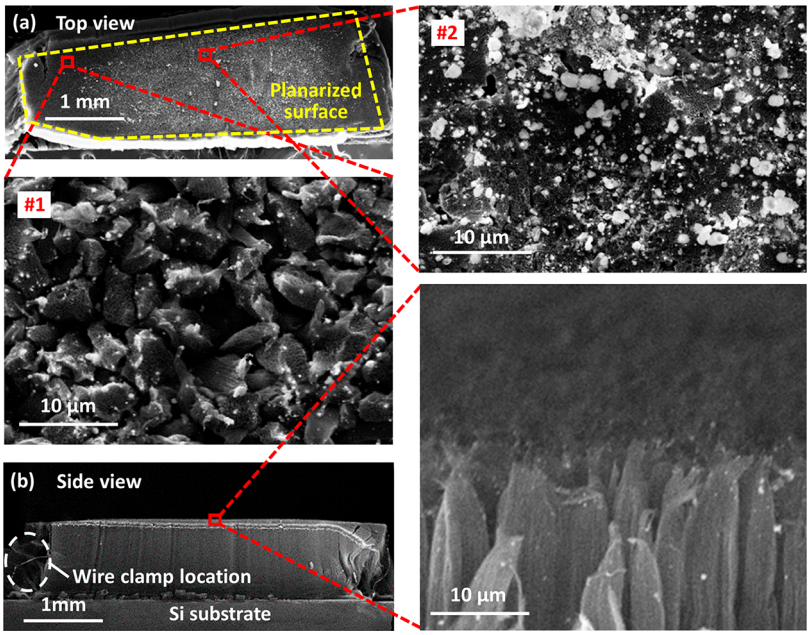

Figure 5. Planarization results for sample no. 2: (a) Top and (b) side views of the sample. The dashed circle in (b) shows the location where the contact copper wire was clamped. Insets nos. 1 and 2 in (a) show detailed views of the top surface of the CNT forest near the side and center locations, respectively. The close-up inset in (b) shows a detailed view of the side surface of the sample.

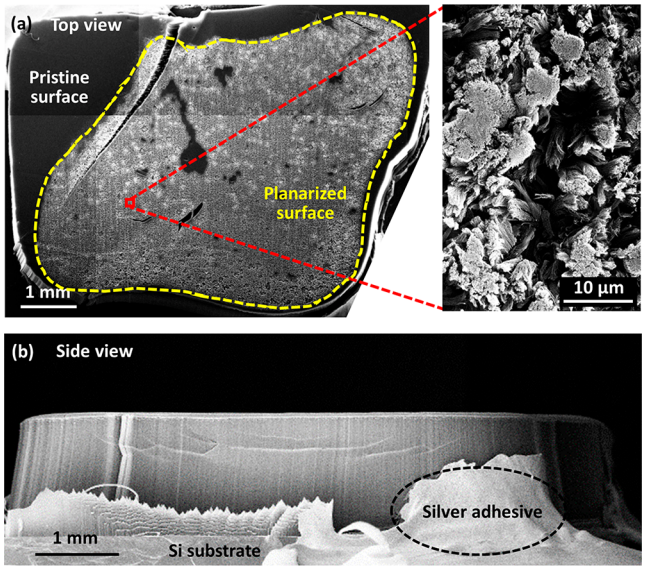

Figure 6. Planarization results for sample no. 3; (a) The top and (b) side view of the sample. The close-up inset in (a) shows a detailed texture of the top surface of the processed sample.

K, and Si K at 0.2770, 0.5100, and 1.7388 keV, respectively. Their corresponding concentrations are tabulated for each measurement result. The presence of oxygen can be attributed to the oxygen molecules trapped with the CNTs in the forest (note that all the samples were kept in air all the time including during the μEDM processes). The silicon signature is assumed to originate from the substrates of the samples as the electron beam can possibly penetrate the CNT forest structure to generate X-rays from the substrate underneath. The concentration of all the elements are similar to those previously reported for μEDMed CNT forest samples.[46]

For sample no. 2, other peaks were identifiable at different energies, that is, Fe L, Ni L, Cr K, and Fe K at energies 0.7048, 0.8530, 5.4140, and 6.4017 keV, respectively. These peaks are a clear signature of the elements of the stainless-steel electrode used. It was observed that the signal levels of these elements depended on the probed site on the top surface. As shown in Figure 7b, the EDX spectrum at a spot near the side of the surface, where no significant amount of debris was found, only included a small signature of Fe L. However, as seen in Figure 7c, all the peaks were identified on a central region of the sample where a large amount of debris was present. The debris produced from μEDM of CNT forest was reported to be comprised of carbon and electrode's material.[47] As mentioned earlier, the presence of debris could have induced abnormal arcing (that presumably led to frequent short circuits and the need for changing electrode's locations with this sample), which could have also enhanced the consumption of the electrode, as discussed in Section 3.2, to leave its byproducts on the sample with an amount detectable by EDX.

The overall structure of sample no. 4 and the process conditions applied for this sample were similar to those for sample no. 1, except that the electrical contact to the CNT forest was made by the wire clamp. Unlike the case of sample no. 1, however, the flattening process of this sample failed; the entire CNT forest was ripped off from the substrate in the middle of the process. Although the exact cause of this outcome is not clear, it may be reasonable to relate it with the sole difference in the process setup, that is, the electrical contact method. The electrical contact with wire clamping could have been weakened while planarizing the sample, especially due to the lateral movement of the sample. Under this condition, the real removal rate could slow and lag behind the feeding rate, which might have narrowed the gap clearance. Simultaneously, similar to the case of sample no. 1, the forest could have been subject to a shear stress (caused by a combination of the lateral motion and the presence of debris) that might have been enhanced by the narrowed gap to eventually cause peeling of the forest. It is also worth noting that the applied voltage causes an electrostatic force to pull the

DOI: 10.1021/acsanm.9b00948
ACS Appl. Nano Mater. 2019, 2, 4594−4604

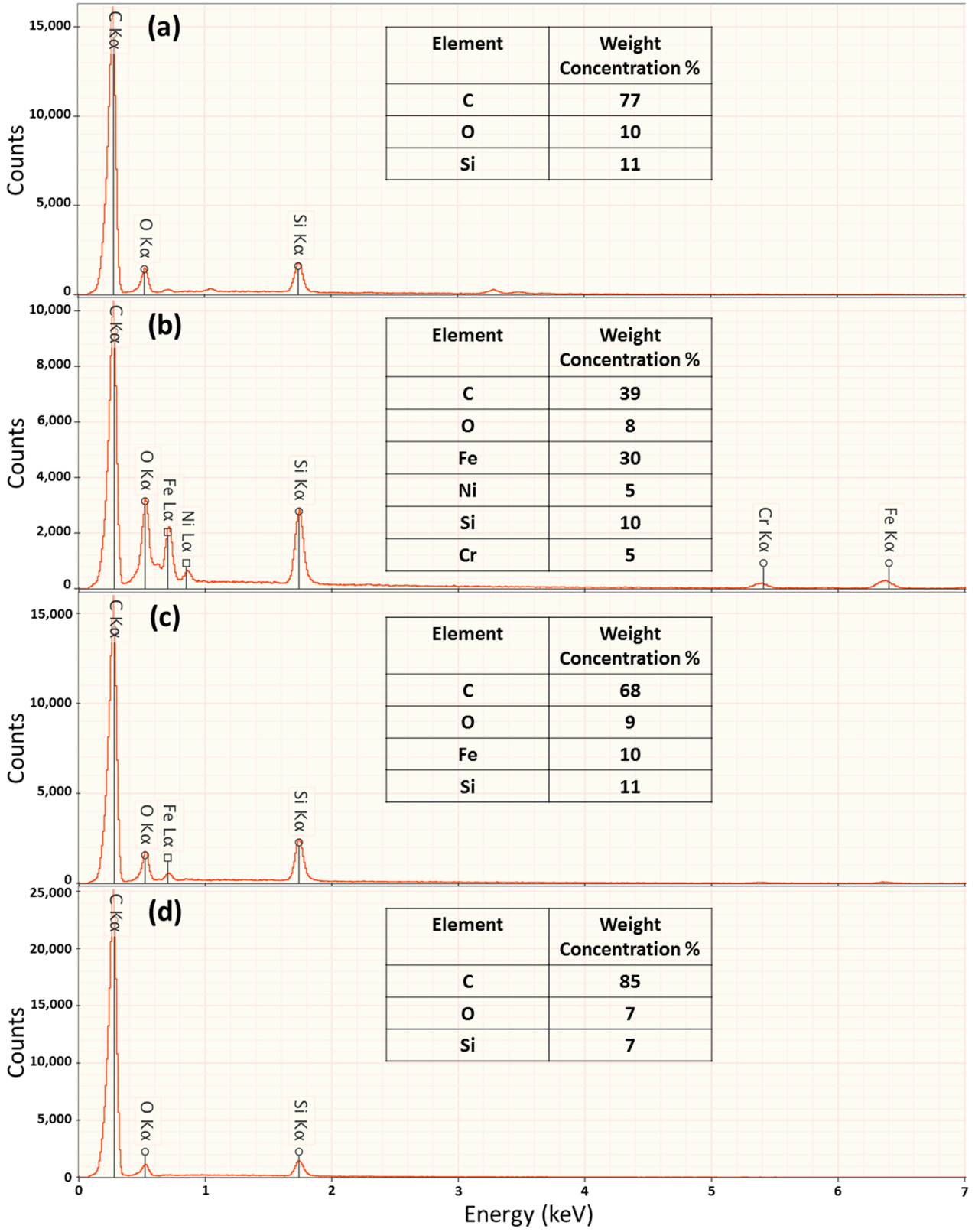

Figure 7. EDX elemental analysis of the planarized surfaces of (a) sample no. 1, (b) sample no. 2 near its perimeter, (c) sample no. 2 at a central location, and (d) sample no. 3. The estimated weight concentrations of major elements are tabulated in each result.

forest up toward the planar electrode, which could have promoted the outcome through the phenomenon known as "pull-in".[56] Besides these external sources, the adhesion of the particular CNT forest to the substrate could have not been strong enough to sustain it against the above forces possibly applied to the forest.

The results from the aforementioned experiments seem to indicate that the electrical contact method plays an important

DOI: 10.1021/acsanm.9b00948
ACS Appl. Nano Mater. 2019, 2, 4594−4604

role in the μEDM planarization of CNT forest. In particular, the use of silver adhesive resulted in a smoother removal process than the case of wire clamping, while showing less debris left on the forest surface after the process. The lateral oscillating motion of the sample under the electrode seems to provide a positive effect on reducing the occurrence of short circuit and irregular discharge. This in turn could suppress debris production and electrode consumption. However, the process for sample no. 3 without the motion also indicated minimal presence of debris on the forest. This result could be related to the potentially greater discharge energy caused by the much larger area or parasitic capacitance associated with the particular forest sample, which could have evaporated CNTs more effectively to leave less debris. The lateral motion was likely the direct cause of the failure in processing sample no. 4. Further study will be necessary for in-depth evaluation of the effect of the motion on the planarization process. Future work will also include the evaluation of characterization methods suitable for large-area quantification of processed CNT forest flatness with high precision including laser confocal microscopy and optical interferometry.

4. CONCLUSION

This study has investigated a postgrowth planarization process for CNT forests using the μEDM method with planar electrodes. The as-grown forest samples, with varying structural dimensions and height nonuniformity, were used to evaluate controlled, parallel-mode removal toward achieving highly uniform top surfaces on them. The flattening process was scaled over large samples with a top surface area of a few 10s of mm^2 and height variations of up to ∼1 mm. The planar removal of the CNT forests was successfully demonstrated to enable several 10-fold improvement in the uniformity of the forest's height, while achieving high parallelism of the top surfaces with their substrates. The analysis of generated discharge pulses revealed a consistent increase in the pulse energy, implying that the parasitic capacitance induced at the interface between the forest's top surface and the electrode increased as the removal area increased during the process. The use of silver conductive adhesive was shown to assist smooth removal processing potentially through a more stable electrical connection between the forest and the discharge circuit compared with the case of mechanical clamping. The obtained results indicate that planar μEDM is a promising postgrowth method for high-precision planarization of CNT forests.

■ ASSOCIATED CONTENT

Supporting Information

The Supporting Information is available free of charge on the ACS Publications website at DOI: 10.1021/acsanm.9b00948.

Postplanarization analysis of planar electrodes and a summary of planarization results (PDF)

■ AUTHOR INFORMATION

Corresponding Authors

*(A.N.) E-mail: anojeh@ece.ubc.ca.
*(K.T.) E-mail: takahata@ece.ubc.ca.

ORCID

Mohab O. Hassan: 0000-0003-0866-1148
Kenichi Takahata: 0000-0001-9637-3677

Author Contributions

The manuscript was written through contributions of all authors. All authors have given approval to the final version of the manuscript.

Notes

The authors declare no competing financial interest.

■ ACKNOWLEDGMENTS

We acknowledge financial support from the Natural Sciences and Engineering Research Council of Canada (Grant Nos. SPG-P 478867 and RGPIN-2017-04608), the Canada Foundation for Innovation, and the British Columbia Knowledge Development Fund. This research was undertaken thanks in part to funding from the Canada First Research Excellence Fund, Quantum Materials and Future Technologies Program.

■ REFERENCES

(1) Saito, R., Dresselhaus, G., Dresselhaus, M. S. *Physical Properties of Carbon Nanotubes*; Imperial College Press: London, 1998.

(2) Ajayan, P. M., Zhou, O. Z. Applications of Carbon Nanotubes. In *Carbon Nanotubes*; Springer: Berlin, Heidelberg, 2001; pp 391–425.

(3) Iijima, S.; Ichihashi, T. Single-shell Carbon Nanotubes of 1-nm Diameter. *Nature* **1993**, *363*, 603.

(4) Baughman, R. H.; Zakhidov, A. A.; De Heer, W. A. Carbon Nanotubes–the Route Toward Applications. *Science* **2002**, *297*, 787–792.

(5) Fan, S.; Chapline, M. G.; Franklin, N. R.; Tombler, T. W.; Cassell, A. M.; Dai, H. Self-oriented regular arrays of carbon nanotubes and their field emission properties. *Science* **1999**, *283*, 512–514.

(6) Murakami, Y.; Chiashi, S.; Miyauchi, Y.; Hu, M.; Ogura, M.; Okubo, T.; Maruyama, S. Growth of Vertically Aligned Single-walled Carbon Nanotube Films on Quartz Substrates and their Optical Anisotropy. *Chem. Phys. Lett.* **2004**, *385*, 298–303.

(7) Qi, H. J.; Teo, K. B. K.; Lau, K. K. S.; Boyce, M. C.; Milne, W. I.; Robertson, J.; Gleason, K. K. Determination of Mechanical Properties of Carbon Nanotubes and Vertically Aligned Carbon Nanotube Forests using Nanoindentation. *J. Mech. Phys. Solids* **2003**, *51*, 2213–2237.

(8) Wirth, C. T.; Hofmann, S.; Robertson, J. Surface Properties of Vertically Aligned Carbon Nanotube Arrays. *Diamond Relat. Mater.* **2008**, *17*, 1518–1524.

(9) Mizuno, K., Ishii, J., Kishida, H., Hayamizu, Y., Yasuda, S., Futaba, D. N., et al. A black body absorber from vertically aligned single-walled carbon nanotubes. In *Proceedings of the National Academy of Sciences*, pnas-0900155106, 2009.

(10) Sohn, J. I.; Lee, S.; Song, Y. H.; Choi, S. Y.; Cho, K. I.; Nam, K. S. Patterned Selective Growth of Carbon Nanotubes and Large Field Emission from Vertically well-Aligned Carbon Nanotube Field Emitter Arrays. *Appl. Phys. Lett.* **2001**, *78*, 901–903.

(11) Chhowalla, M.; Teo, K. B. K.; Ducati, C.; Rupesinghe, N. L.; Amaratunga, G. A. J.; Ferrari, A. C.; et al. Growth Process Conditions of Vertically Aligned Carbon Nanotubes using Plasma Enhanced Chemical Vapor Deposition. *J. Appl. Phys.* **2001**, *90*, 5308–5317.

(12) Ren, Z. F.; Huang, Z. P.; Xu, J. W.; Wang, J. H.; Bush, P.; Siegal, M. P.; Provencio, P. N. Synthesis of Large Arrays of well-Aligned Carbon Nanotubes on Glass. *Science* **1998**, *282*, 1105–1107.

(13) Lee, C. J.; Kim, D. W.; Lee, T. J.; Choi, Y. C.; Park, Y. S.; Lee, Y. H.; et al. Synthesis of Aligned Carbon Nanotubes using Thermal Chemical Vapor Deposition. *Chem. Phys. Lett.* **1999**, *312*, 461–468.

(14) Hart, A. J.; Slocum, A. H. Rapid Growth and Flow-mediated Nucleation of Millimeter-scale Aligned Carbon Nanotube Structures from a Thin-film Catalyst. *J. Phys. Chem. B* **2006**, *110*, 8250–8257.

(15) Bedewy, M.; Farmer, B.; Hart, A. J. Synergetic Chemical Coupling Controls the Uniformity of Carbon Nanotube Microstructure Growth. *ACS Nano* **2014**, *8*, 5799–5812.

DOI: 10.1021/acsanm.9b00948
ACS Appl. Nano Mater. 2019, 2, 4594–4604

(16) Jeong, G. H.; Olofsson, N.; Falk, L. K.; Campbell, E. E. Effect of Catalyst Pattern Geometry on the Growth of Vertically Aligned Carbon Nanotube Arrays. *Carbon* **2009**, *47*, 696−704.
(17) Hutchens, S. B.; Hall, L. J.; Greer, J. R. In situ Mechanical Testing reveals Periodic Buckle Nucleation and Propagation in Carbon Nanotube Bundles. *Adv. Funct. Mater.* **2010**, *20*, 2338−2346.
(18) De Volder, M., Tawfick, S., Hart, A. J. Controlled growth orientation of carbon nanotube pillars by catalyst patterning in microtrenches. In *Solid-State Sensors, Actuators and Microsystems Conference, 2009. TRANSDUCERS 2009. International*; IEEE, June, 2009; pp 2046−2049.
(19) Lin, A.; Patil, N.; Ryu, K.; Badmaev, A.; De Arco, L. G.; Zhou, C.; et al. Threshold Voltage and on-off Ratio Tuning for Multiple-tube Carbon Nanotube FETs. *IEEE Trans. Nanotechnol.* **2009**, *8*, 4.
(20) Hata, K.; Futaba, D. N.; Mizuno, K.; Namai, T.; Yumura, M.; Iijima, S. Water-assisted Highly Efficient Synthesis of Impurity-free Single-walled Carbon Nanotubes. *Science* **2004**, *306*, 1362−1364.
(21) Han, J. H.; Graff, R. A.; Welch, B.; Marsh, C. P.; Franks, R.; Strano, M. S. A Mechanochemical Model of Growth Termination in Vertical Carbon Nanotube Forests. *ACS Nano* **2008**, *2*, 53−60.
(22) Ya'akobovitz, A.; Bedewy, M.; Hart, A. J. Electrostatic Capacitance and Faraday cage Behavior of Carbon Nanotube Forests. *Appl. Phys. Lett.* **2015**, *106*, 053106.
(23) Jiang, Y. Q., Zhou, Q., Lin, L. Planar MEMS supercapacitor using carbon nanotube forests. In *Micro Electro Mechanical Systems, 2009. MEMS 2009. IEEE 22nd International Conference on*; IEEE, January, 2009; pp 587−590.
(24) Futaba, D. N.; Hata, K.; Yamada, T.; Hiraoka, T.; Hayamizu, Y.; Kakudate, Y.; et al. Shape-engineerable and Highly Densely packed Single-walled Carbon Nanotubes and their Application as Super-capacitor Electrodes. *Nat. Mater.* **2006**, *5*, 987.
(25) Choi, J.; Lee, J. I.; Eun, Y.; Kim, M. O.; Kim, J. Aligned Carbon Nanotube Arrays for Degradation-Resistant, Intimate Contact in Micromechanical Devices. *Adv. Mater.* **2011**, *23*, 2231−2236.
(26) Olofsson, N.; Ek-Weis, J.; Eriksson, A.; Idda, T.; Campbell, E. E. Determination of the effective Young's modulus of Vertically Aligned Carbon Nanotube Arrays: a simple nanotube-based varactor. *Nanotechnology* **2009**, *20*, 385710.
(27) Yaghoobi, P.; Moghaddam, M. V.; Nojeh, A. Heat trap": Light-induced Localized Heating and Thermionic Electron Emission from Carbon Nanotube Arrays. *Solid State Commun.* **2011**, *151*, 1105−1108.
(28) Lee, J. H.; Bargatin, I.; Melosh, N. A.; Howe, R. T. Optimal Emitter-Collector Gap for Thermionic Energy Converters. *Appl. Phys. Lett.* **2012**, *100*, 173904.
(29) Li, Z.; Bai, B.; Li, C.; Dai, Q. Efficient Photo-thermionic Emission from Carbon Nanotube Arrays. *Carbon* **2016**, *96*, 641−646.
(30) Li, C.; Li, Z.; Chen, K.; Bai, B.; Dai, Q. Edge effect Enhanced Photo-thermionic Emission from a Carbon Nanotubes Array. *Appl. Phys. Lett.* **2017**, *110*, 093105.
(31) Voon, K., Dridi, K., Chowdhury, M., Chang, M., Nojeh, A. The Role of carbon nanotube forest density in thermionic emission. In *Vacuum Nanoelectronics Conference (IVNC), 2016 29th International*; IEEE, July, 2016; pp 1−2.
(32) Bedewy, M.; Meshot, E. R.; Reinker, M. J.; Hart, A. J. Population Growth Dynamics of Carbon Nanotubes. *ACS Nano* **2011**, *5*, 8974−8989.
(33) Yasuda, S.; Futaba, D. N.; Yamada, T.; Satou, J.; Shibuya, A.; Takai, H.; et al. Improved and Large Area Single-walled Carbon Nanotube Forest Growth by Controlling the Gas Flow Direction. *ACS Nano* **2009**, *3*, 4164−4170.
(34) Cheong, F. C.; Lim, K. Y.; Sow, C. H.; Lin, J.; Ong, C. K. Large Area Patterned Arrays of Aligned Carbon Nanotubes via Laser Trimming. *Nanotechnology* **2003**, *14*, 433.
(35) Lim, K. Y.; Sow, C. H.; Lin, J.; Cheong, F. C.; Shen, Z. X.; Thong, J. T. L.; et al. Laser Pruning of Carbon Nanotubes as a Route to Static and Movable Structures. *Adv. Mater.* **2003**, *15*, 300−303.
(36) Wang, T.; Jiang, D.; Chen, S.; Jeppson, K.; Ye, L.; Liu, J. Formation of three-dimensional Carbon Nanotube Structures by Controllable Vapor Densification. *Mater. Lett.* **2012**, *78*, 184−187.
(37) Jiang, D.; Wang, T.; Chen, S.; Ye, L.; Liu, J. Mediated Controlled Densification and Low Temperature Transfer of Carbon Nanotube Forests for Electronic Interconnect Application. *Microelectron. Eng.* **2013**, *103*, 177−180.
(38) Masaki, T., Kawata, K., Masuzawa, T. Micro electro-discharge machining and its applications. In *Micro Electro Mechanical Systems, 1990. Proceedings, An Investigation of Micro Structures, Sensors, Actuators, Machines and Robots*; IEEE, February, 1990; pp 21−26.
(39) Fofonoff, T. A.; Martel, S. M.; Hatsopoulos, N. G.; Donoghue, J. P.; Hunter, I. W. Microelectrode Array Fabrication by Electrical Discharge Machining and Chemical Etching. *IEEE Trans. Biomed. Eng.* **2004**, *51*, 890−895.
(40) Takahata, K.; Gianchandani, Y. B.; Wise, K. D. Micromachined Antenna Stents and Cuffs for Monitoring Intraluminal Pressure and Flow. *J. Microelectromech. Syst.* **2006**, *15*, 1289−1298.
(41) Jahan, M. P.; Rahman, M.; Wong, Y. S. A Review on the Conventional and Micro-Electrodischarge Machining of Tungsten Carbide. *International Journal of Machine Tools and Manufacture* **2011**, *51*, 837−858.
(42) Ehrfeld, W., Lehr, H., Michel, F., Wolf, A., Gruber, H. P., Bertholds, A. Microelectro discharge machining as a technology in micromachining. In *Micromachining and Microfabrication Process Technology II*; International Society for Optics and Photonics, September, 1996; Vol. *2879*, pp 332−338.
(43) Takahata, K. Micro-Electro-Discharge Machining Technologies for MEMS. In *Micro Electronic and Mechanical Systems*; InTech, 2009.
(44) Xiao, Z.; Dahmardeh, M.; Moghaddam, M. V.; Nojeh, A.; Takahata, K. Scaling Approach toward Nano Electro-Discharge Machining: Nanoscale Patterning of Carbon Nanotube Forests. *Microelectron. Eng.* **2016**, *150*, 64−70.
(45) Xiao, Z.; Saquib Sarwar, M.; Dahmardeh, M.; Vahdani Moghaddam, M.; Nojeh, A.; Takahata, K. Cone-shaped Forest of Aligned Carbon Nanotubes: An Alternative Probe for Scanning Microscopy. *Appl. Phys. Lett.* **2013**, *103*, 171603.
(46) Sarwar, M. S.; Dahmardeh, M.; Nojeh, A.; Takahata, K. Batch-mode Micropatterning of Carbon Nanotube Forests using UV-LIGA assisted Micro-Electro-Discharge Machining. *J. Mater. Process. Technol.* **2014**, *214*, 2537−2544.
(47) Khalid, W.; Ali, M. S. M.; Dahmardeh, M.; Choi, Y.; Yaghoobi, P.; Nojeh, A.; Takahata, K. High-aspect-ratio, Free-form Patterning of Carbon Nanotube Forests using Micro-Electro-Discharge Machining. *Diamond Relat. Mater.* **2010**, *19*, 1405−1410.
(48) Park, J. W.; Kim, B. H.; Ok, J. G.; Kim, W. J.; Kim, Y. H.; Chu, C. N. Wire Electrical Discharge Machining of Carbon Nanofiber Mats for Field Emission. *International Journal of Precision Engineering and Manufacturing* **2012**, *13*, 593−599.
(49) Liang, B.; Ogino, A.; Nagatsu, M. Discharge Characteristics of a Nano-sized Electrode with Aligned Carbon Nanotubes grown on a Tungsten Whisker Tip under various Gas Conditions. *J. Phys. D: Appl. Phys.* **2010**, *43*, 275202.
(50) Ok, J. G.; Kim, B. H.; Sung, W. Y.; Lee, S. M.; Lee, S. W.; Kim, W. J.; et al. Electrical Discharge Machining of Carbon Nanomaterials in Air: Machining Characteristics and the Advanced Field Emission Applications. *J. Micromech. Microeng.* **2008**, *18*, 025007.
(51) Dahmardeh, M.; Vahdani Moghaddam, M.; Hian Tee, M.; Nojeh, A.; Takahata, K. The Effects of three-dimensional Shaping of Vertically Aligned Carbon-Nanotube Contacts for Micro-Electro-Mechanical Switches. *Appl. Phys. Lett.* **2013**, *103*, 231606.
(52) Saleh, T.; Dahmardeh, M.; Nojeh, A.; Takahata, K. Dry Micro-Electro-Discharge Machining of Carbon-Nanotube Forests using Sulphur-hexafluoride. *Carbon* **2013**, *52*, 288−295.
(53) Vahdani Moghaddam, M.; Yaghoobi, P.; Nojeh, A. Polarization-dependent Light-induced Thermionic Electron Emission from Carbon Nanotube Arrays using a wide range of Wavelengths. *Appl. Phys. Lett.* **2012**, *101*, 253110.

DOI: 10.1021/acsanm.9b00948
ACS Appl. Nano Mater. 2019, 2, 4594−4604

(54) Murray, J. W.; Sun, J.; Patil, D. V.; Wood, T. A.; Clare, A. T. Physical and Electrical Characteristics of EDM Debris. *J. Mater. Process. Technol.* **2016**, *229*, 54−60.
(55) Dahmardeh, M.; Nojeh, A.; Takahata, K. Possible Mechanism in Dry Micro-Electro-Discharge Machining of Carbon-Nanotube Forests: A Study of the Effect of Oxygen. *J. Appl. Phys.* **2011**, *109*, 093308.
(56) Pamidighantam, S.; Puers, R.; Baert, K.; Tilmans, H. A. Pull-in Voltage Analysis of Electrostatically Actuated Beam Structures with fixed−fixed and fixed−free end Conditions. *Journal of Micromechanics and Microengineering* **2002**, *12*, 458.

DOI: 10.1021/acsanm.9b00948
ACS Appl. Nano Mater. 2019, 2, 4594−4604